Uncovering Interactions in Frequency Domains

Shuixia Guo[1] Jianhua Wu[3] Mingzhou Ding[2] Jianfeng Feng[1,3]

[1]Department of Mathematics, Hunan Normal University, Changsha 410081, P.R.China

[2] J Crayton Pruitt Family Dept Biomed Engn, Univ Florida, Gainesville, FL 32611 USA

[3]Department of Computer Science and Mathematics, Warwick University, Coventry CV4 7AL, UK

February 8, 2008

Abstract

Oscillatory activity plays a critical role in regulating biological processes ranging from subcellular, cellular, network to whole organism. We shed lights on this issue by introducing a novel approach called partial Granger causality to reliably reveal interactions in the data with exogenous inputs and latent variables in the frequency domain. The method is extensively tested with toy models, and is successfully applied to experimental data sets, including gene microarray data of HeLa cell cycle; intra-network data–*in vivo* multi-electrode array (MEA) local field potentials (LFPs) recorded from the inferotemporal cortex of sheep; and inter-network data–*in vivo* local field potentials (LFPs) recorded from macaque monkeys using bipolar electrodes at different distributed sites in multiple cortical areas of the right hemisphere in monkey.

1 Introduction

Recently, as reviewed in [30], many novel approaches in molecular biology have been invented to improve the bulk-scale methods that measure average values for a population of genes or proteins and mask their dynamical activities which are critical for the function of cells [19, 29, 32]. On the other hand, in neurophysiology, there is a long history of dynamically recording single neuron, neuronal network and brain area activities. Based upon such experimental data, to explore the network structure of genes, proteins, neurons etc is one of the most important issues in System Biology. As such, in the literature, there exist two closely intermingling approaches (see for example [10, 7, 9, 33]) to tackle the problem: Bayesian approach and Granger approach. The appealing properties of the Granger causality approach are

- the causal relationship is a clear indication of time;
- there is a corresponding frequency decomposition which clearly shows at which frequency two units or variables interact with each other.

In the current paper we concentrate on the Granger causality approach. The concept of the Granger causality originally introduced by Wiener [35] and formulated by Granger [14] has played a considerably important role in investigating the relationship among stationary time series. Specifically, given two time series, if the variance of the prediction error for the second time series at the present time is reduced by including past measurements from the first time series in the (non)linear regression model, then the first time series can be said to cause the second time series. Geweke's decomposition of a vector autoregressive process [11] led to a set of causality measures which have a spectral representation and make the interpretation more informative and useful[22].

We first develop a novel approach to calculate Granger causality: partial Granger causality, both in time and frequency domains, aiming to deal with the case that the data recorded has latent variables. In toy models we compare our approach with partial directed coherence (PDC) which is used to detect direct influence of multivariables and is thought of to be the best theoretical framework for spectral analysis of linear multidimensional coupling

up to date[17]. It might not be too surprising to see that our definition clearly picks up the right causal relationship, but PDC fails (see Fig. 2). The simple reason is that our decomposition relies on the Kolmogrov equation, but PDC type approach lacks this property. As a consequence, a frequency domain decomposition could be simply in contradiction with the obtained conclusions in the time domain.

We then apply our approach to three sets of experimental data. In the first one, the data is obtained from microarray data of HeLa cell [34], involving IκB–NF-κB circuit. Although the data has been widely analyzed in the literature, it seems that no results have been reported in the frequency domains. Our approach clearly reveals three basic frequencies in the circuit. The first one corresponding to 16-hour period is the HeLa cycle time. The second one is around 4-hour period which has been reported in [19, 29]. Finally the third is around 10-hour and is reported in other gene networks such as P53 network[30]. Our causality analysis tells us how these genes interact with each other at different frequencies and IκB–NF-κB circuit is a tri-frequency circuit. We then turn our attention to multi-electrode array recordings from behaving sheep's inferotemporal cortex (IT) when it performs a discriminant task. A small subset (five channels) of all recordings is used in our analysis to illustrate the application of our approach. The third set of data is recorded from a monkey named GE using transcortical bipolar electrodes at 15 distributed sites in multiple cortical areas of the right hemisphere. In comparison with the results obtained from the conditional Granger causality, an additional interaction between two areas is found.

2 Results

2.1 Toy models

To illustrate the frequency decomposition of the partial Granger causality introduced here, we first consider a toy model with exogenous inputs and latent variables (see Methods section).

Example 1 Suppose that 5 simultaneously generated time series are defined by the equa-

tions

$$\begin{cases} x_1(t) &= 0.95\sqrt{2}x_1(t-1) - 0.9025x_1(t-2) + \epsilon_1(t) + a_1\epsilon_6(t) \\ & \quad +b_1\epsilon_7(t-1) + c_1\epsilon_7(t-2) \\ x_2(t) &= 0.5x_1(t-2) + \epsilon_2(t) + a_2\epsilon_6(t) + b_2\epsilon_7(t-1) + c_2\epsilon_7(t-2) \\ x_3(t) &= -0.4x_1(t-3) + \epsilon_3(t) + a_3\epsilon_6(t) + b_3\epsilon_7(t-1) + c_3\epsilon_7(t-2) \\ x_4(t) &= -0.5x_1(t-2) + 0.25\sqrt{2}x_4(t-1) + 0.25\sqrt{2}x_5(t-1) + \epsilon_4(t) \\ & \quad +a_4\epsilon_6(t) + b_4\epsilon_7(t-1) + c_4\epsilon_7(t-2) \\ x_5(t) &= -0.25\sqrt{2}x_4(t-1) + 0.25\sqrt{2}x_5(t-1) + \epsilon_5(t) + a_5\epsilon_6(t) \\ & \quad +b_5\epsilon_7(t-1) + c_5\epsilon_7(t-2) \end{cases}$$

where $\epsilon_i(t), i = 1, 2, \cdots, 7$ are zero-mean uncorrelated process with an identical variance. $a_i\epsilon_6$ is the exogenous input and the term $b_i\epsilon_7(t-1) + c_i\epsilon_7(t-2)$ represents the influence of latent variables.

From the model, one can see that $x_1(t)$ is a direct source to $x_2(t), x_3(t)$, and $x_4(t)$, $x_4(t)$ and $x_5(t)$ share a feedback loop and there is no direct connection between $x_1(t)$ and $x_5(t)$. We perform a simulation of this system with $a_i \sim U[0,1], b_i = 2, c_i = 5, i = 1, \cdots, 5$ (we extensively tested our approach in other more general cases of a_i, b_i, c_i, see [17]) to generate a data set of 2000 data points with a sample rate of 200 Hz. Fig. 1 (**A**) illustrates the traces of 5 time series. It is obvious that the system is stationary. The network structure is depicted in Fig. 1 (**B**). Fig. 1 (**C**) is the comparison between our partial Granger causality $F^{(1)}$ and the conditional Granger causality $F^{(2)}$ [6]. It is clearly shown that our partial Granger causality outperforms the conditional Granger causality. The values of the conditional Granger causality are all very small due to the latent variables and common inputs, while the correct structure is revealed via the partial Granger causality. In particular, the interaction $4 \rightarrow 5$ is not picked out by the conditional causality, but it is correctly revealed in our partial Granger causality approach.

Fig. 1 around here

Fig. 1 (**D**) presents a comparison between the time domain partial Granger causality and the frequency domain partial Granger causality. Blue line is the value of the partial Granger causality for all 20 kinds of relationship calculated in the time domain. Red line is the summation (integration) of the partial Granger causality for frequencies in the range

of $[-\pi, \pi]$. As expected, Fig. 1 (**D**) demonstrates that the decomposition in the frequency domain fits very well with the partial Granger causality in the time domain.

As mentioned before, PDC is supposed to be the best quantity up to date in the literature to reveal the causal relationship in the frequency domain [17]. However, it lacks a theoretical background. Fig. 2 is the detailed comparison of the causality in the frequency domain of all 20 kinds of relationship between the partial Granger causality(PGC) and PDC. The upper panels are the results obtained from the PGC in the frequency domain. It is easy to see that there are direct causal drives from 1 to 2,3 and 4, and a feedback between 5 and 4. Most importantly it is consistent with the results in the time domain. The bottom panels are the results obtained from PDC. It is evident that the causality for almost all relationship is significant, in contradiction with the results in the time domain.

Fig. 2 around here

We have extensively tested the PGC and compared it with existing approaches [16], although only a very special case is reported here. Next we apply PGC to experimental data.

2.2 NF-κB: A tri-frequency circuit

We applied partial causality analysis to HeLa cell cycle gene expression data collected by Whitfield et al. (2002)[34]. These data contain three complete cell cycles, i.e., 48 time points distributed at intervals of 1h, where the HeLa cell cycle is 16h. This data can be downloaded at: http://genome-www.stanford.edu/Human-CellCycle/Hela/. At each time point, there are three or four replicates for each gene selected.

The NF-κB, a stress-regulated transcription factor belonging to the Rel family, plays a pivotal role in the control of inflammatory and innate responses. NF-κB activation has been related to multiple aspects of tumorigenesis, including the control of cell proliferation and migration, cell cycle progression and apoptosis. Whereas only limited information is available regarding the direct involvement of NF-κB in cell-cycle regulation, it was also found that the levels of NF-B activation are linked to signaling that controls cell-cycle progression in HeLa cells.

Here we applied pairwise Granger causality method and partial Granger causality (PGC) methods based on a sliding-window VAR model. We only applied both methods to one typical gene modules, which is regulated by 2 transcription factors, namely: nuclear factor-κB (NF-κB) in the context of cell cycle progression of transformed HeLa cells. In Fig. 3 (**A**), we plotted the original data and fitted VAR model (dotted lines). The obtained results of Granger causality in the time domain are depicted in Fig. 3 (**B**) (pairwise Granger causality) and in Fig. 3 (**C**) (PGC).

Our gene expression analysis (Fig. 3) indicates that the activation of NF-κB correlates with increased activity of IKKα, a natural repressor of IκB-dependent inhibition of NF-κB. As presented in Fig.3 (**B**), for the causal network of NF-κB module based on pairwise Granger causality analysis there are directional connections between IKKα, NEMO and IκB, and also bidirectional connections between IKKα, IκB and NF-κB. Here only the causality that is significant is shown, and the magnitude of the causality and the confidence interval are presented along the arrows. Fig.3 (**C**) shows the causal network of NF-κB module based on partial Granger causality analysis presented in this paper. Four directional causality connections are preserved and two are eliminated after partial causality analysis is applied. As reported by experimental data, the activity of NF-κB is tightly regulated by its interaction with inhibitory IκB proteins. Activation of NF-κB is achieved through the action of a family of serine/threonine k (IKK). The IKK contains two catalytic subunits (IKKα and IKKβ) and a regulatory/adapter protein NEMO (also known as IKKγ). The causality analysis of NF-κB module presents the activation progression of NF-κB, and it also depicts the causal effect of each gene during the transcription progression. The results indicate that NF-κB transcription factor participates (directly or indirectly) in the control of a complex pattern of HeLa cell cycle regulators in a bidirectional fashion.

Fig. 3 around here

As discussed in Method section, the Granger causality is consistent in both time and frequency domains. However, it may be more convenient to project the time domain causality into frequency domain causality, such that the profile connections can be examined under a specific frequency. Fig. 3 (**D**) presents the power spectrum plot for four genes. The power of the four gene concentrate on three specific frequencies $f_1 = 0.061, f_2 = 0.11$ and

$f_3 = 0.22\ h^{-1}$. Then partial frequency causality in the frequency domain is calculated.

It is interesting to see that the peak of IKKα $\rightarrow$NEMO is around 16 hours, which implies that the HeLa cell cycle is originated from the driving of IKKα. The peak causality of NEMO$\rightarrow$IκB is at 10 hours. Although the power at 10-hour frequency is less that the other two, but it is consistently presented in all genes. To the best of our knowledge, it seems there are no direct reports on the 10-hour frequency of the NF-κB circuit. However, it is reported in, for example, p53 circuit (see Fig. 1 (**A**) in [30]). The important role played by NF-κB to regulate p53 circuit has been reported in [26]. The second peak of NEMO$\rightarrow$IκB locates at around 4-hour frequency and PSD is very significant in both NEMO and IκB. This frequency is reported in, for example, Fig. 2 in [29]. From our analysis, we conclude that the 4-hour frequency is generated from NEMO, but it is absent in IKKα. It would be interesting to test this experimentally and single out its functional meaning. Furthermore, the driving from IκB to NF-κB is mainly at 16-hour frequency and its harmonic (8-hour) frequency. Finally the feedback from NF-κB to IκB is less frequency specific.

2.3 Intra-network data: theta-frequency circuit

The experimental data set is the local field potential (LFP) data that was collected from the left and right hemisphere of the sheep inferotemporal cortex. Multi-electrode array recordings consisted of 64 channels in each hemisphere and individual electrodes were fabricated from tungsten wires (125μ diam.) sharpened to a tip smaller than 1μ and insulated with epoxylite. The sampling frequency for the LFPs were 2000 Hz. The sheep were trained to perform an operant discrimination task in which different pairs of sheep faces were presented and a correct panel-press response elicited a food reward[20, 21, 36, 37, 38].

Inferior temporal (IT) cortex is considered to be the highest processing stage alongside the ventral pathway. It is involved with higher cognitive functions such as categorisation and memory formation. fMRI study has reported ventral temporal regions of primates can be differently activated by different visual stimuli, such as faces, houses and other objects [24]. Recently both spikes and local field potentials have been found to be selective to a variety of stimuli and they are tolerant to retinal position and size [25].

Much of current studies are based on either neuroimaging or single unit recording techniques. fMRI can accurately locate the brain regions that are active during a visual task but its temporal resolution is poor. Single unit recordings provide direct detailed neuronal information but it is unable to investigate large neuronal ensembles. We use multi-electrode array that consists of up to 128 electrodes and make recordings in sheep IT cortex in both brain hemispheres while animals performed discrimination tasks between pairs of faces and objects (see Fig. 4 (**A**)).

To see the spatial power distribution on the recording array, the electrodes with increased theta power were arranged by the latency of each channel. Fig .4 (**B**)shows the theta (3-10Hz) power distribution on the electrode array. The activation of theta power for face stimuli is concentrated within the latency of 300-350ms activating region of the second half of the left hemisphere and nearly the whole area of the right hemisphere. The activation region for object presentation is similar on its topographical positions of the array but it elicits a sequential latency pattern with a major activation starting at 200 ms in the left hemisphere preceding the 250 ms activation in the right. Sequential activation is also observed for face stimuli in other recording sessions. If considering that LFP carries input signals from previous layers, synchronised theta wave may represent a parallel input into IT while sequence of theta waves with different latencies may also present the phenomena of the travelling waves within the recorded region.

Ideally, it would be great if we could find all links between all channels (64 channels). However, even with the data size we have at moment (10 seconds recordings with a sample rate of 2K Hz), to first fit them with a 64 dimensional time series is somewhat problematic. Hence, here we only select five channels to demonstrate the application of our approach and will publish the biological results elsewhere. The links revealed in our approach could be thought of as 'functional' interactions between five channels, as in the fMRI literature[28]. Certainly the data would fit well with the setup of the current paper: it contains the exogenous input (see below) and latent variables (due to unrecorded inputs and the fact that we only choose five channels).

Fig. 4 around here

In Fig. 4 (**C**), the obtained partial Granger causality in the time domain is shown.

The complete causal relationship is presented in Fig. 4 (**D**). In Fig. 4 (**E**), the partial Granger causality in the frequency domain is depicted. We conclude that the interaction between these channels is at the theta band. For example, the frequency decomposition corresponding to the peak (1→4) in Fig. 4(**C**) in the time domain has a peak around 10 Hz. Although there are activities in the power spectral density in the gamma band for the five channels (not shown), we have not observed any interactions between these five channels.

2.4 Inter-network data: beta- and gamma-frequency circuit

We refer the reader to [6] for details of the data description. LFP were collected when monkey performed a GO/NO-GO visual pattern discrimination task. The presence of oscillatory field potential activity in the beta (14-30Hz) frequency range was reported in the sensorimotor cortex of the monkey during the prestimulus period.

It is pointed out in [6] that if only pairwise Granger causality is applied, the obtained structure is as depicted in Fig. 5 (**A**). Using the conditional Granger causality, the causal relationship between the primary somatosensory (S1) and one of the inferior posterior parietal site (in area 7a) is eliminated. Applying the partial Granger causality in the time domain, we obtain the results as shown in Fig. 5 (**B**) where the actual values and the confidence intervals are depicted. 7b is another inferior posterior parietal site and M1 is the primary motor site. It is clearly seen that there are six causal relationships, i.e., S1→M1, 7b→M1, 7b→S1, 7b→7a, S1→7b and finally 7a→7b. Fig. 5 (**C**) is the Granger causality in the frequency domain. According to Fig. 5 (**B**), we see that there are six pairs which have significant Granger causality. The first five have been reported in the literature and are in the Beta band (10-30)Hz. The final one, 7a→7b, has a peak at a high frequency (the supper Gamma band). It has been reported in the literature that the nervous systems use different frequency bands to communicate with each other[4].

3 Methods

3.1 Partial Granger causality: time domain

Consider a multiple stationary time series of dimension n, $\{W_t\}$. The series has the following vector autoregressive representation with the use of the lag operator $\mathcal{L}$:

$$\mathbf{B}(\mathcal{L})W_t = \xi_t, \tag{1}$$

where $E(\xi_t) = \mathbf{0}, \text{var}(\xi_t) = \mathbf{\Sigma}$, an $n \times n$ matrix, and $\mathbf{B}$ is a polynomial matrix of $\mathcal{L}$. $\mathbf{B}(0) = \mathbf{I}_n$, the $n \times n$ identity matrix. Now suppose that W_t has been decomposed into three vectors (measured variables) X_t, Y_t and Z_t with k, l and m dimensions, respectively, i.e. $W_t = (X_t^T, Y_t^T, Z_t^T)^T$, where $(\cdot)^T$ denotes matrix transposition.

Generally, the perturbation ξ_t in eq. (1) can be represented as a noise term ϵ_t together with an exogenous term E_t^x and a latent variable term L_t^a [1] , then eq. (1) can be rewritten as

$$\mathbf{B}(\mathcal{L})W_t = E_t^x + \epsilon_t + L_t^a, \tag{2}$$

where the random vectors (E_t^x, L_t^a) and ϵ_t are independent. The exogenous variable E_t^x represents the environmental drive and is typically present in any experimental setup. For example, all neurons in the inferior temporal cortex receive inputs from its preceding layers (visual cortex) and the incoming signal could be represented by exogenous variables. The latent variable L_t^a are variables which can not be measured in the experiment.

The vector autoregressive representation for W involving three time series X_t (k dimensional vector), Y_t (l dimensional vector) and Z_t (m dimensional vector) can be written in the following way.

$$\begin{cases} X_t &= \sum_{i=1}^{\infty} a_{1i}X_{t-i} + \sum_{i=1}^{\infty} b_{1i}Y_{t-i} + \sum_{i=1}^{\infty} c_{1i}Z_{t-i} + \overrightarrow{\epsilon_{1t}} + \overrightarrow{\epsilon_{1t}^E} + \overrightarrow{B_1(\mathcal{L})\epsilon_{1t}^L} \\ Y_t &= \sum_{i=1}^{\infty} d_{1i}X_{t-i} + \sum_{i=1}^{\infty} e_{1i}Y_{t-i} + \sum_{i=1}^{\infty} f_{1i}Z_{t-i} + \overrightarrow{\epsilon_{2t}} + \overrightarrow{\epsilon_{2t}^E} + \overrightarrow{B_2(\mathcal{L})\epsilon_{2t}^L} \\ Z_t &= \sum_{i=1}^{\infty} g_{1i}X_{t-i} + \sum_{i=1}^{\infty} h_{1i}Y_{t-i} + \sum_{i=1}^{\infty} k_{1i}Z_{t-i} + \overrightarrow{\epsilon_{3t}} + \overrightarrow{\epsilon_{3t}^E} + \overrightarrow{B_3(\mathcal{L})\epsilon_{3t}^L} \end{cases} \tag{3}$$

[1] Due to Wald representation, latent variables can be represented as the summation of normally distributed random inputs, depending on history.

where $\overrightarrow{\epsilon_{it}}, \overrightarrow{\epsilon_{it}^{E}}, \overrightarrow{\epsilon_{it}^{L}}$ are normally distributed random vectors and $B_i(\mathcal{L})$ is a polynomial matrix of $\mathcal{L}$ of appropriate size.

For simplicity of notation, let us define

$$u_i(t) = \overrightarrow{\epsilon_{it}} + \overrightarrow{\epsilon_{it}^{E}} + \overrightarrow{B_i(\mathcal{L})\epsilon_{it}^{L}}$$

$i = 1, 2, 3$. The noise covariance matrix for eq. (3) can be represented as

$$\Sigma = \begin{bmatrix} \text{var}(u_{1t}) & \text{cov}(u_{1t}, u_{2t}) & \text{cov}(u_{1t}, u_{3t}) \\ \text{cov}(u_{2t}, u_{1t}) & \text{var}(u_{2t}) & \text{cov}(u_{2t}, u_{3t}) \\ \text{cov}(u_{3t}, u_{1t}) & \text{cov}(u_{3t}, u_{2t}) & \text{var}(u_{3t}) \end{bmatrix} = \begin{bmatrix} \Sigma_{xx} & \Sigma_{xy} & \Sigma_{xz} \\ \Sigma_{yx} & \Sigma_{yy} & \Sigma_{yz} \\ \Sigma_{zx} & \Sigma_{zy} & \Sigma_{zz} \end{bmatrix}$$

Following the idea of defining Granger causality, let us further consider two time series X_t and Z_t (to fit X_t and Z_t in W exclusively using X and Z), the joint autoregressive representation for X_t and Z_t can be written as

$$\begin{cases} X_t &= \sum_{i=1}^{\infty} a_{2i} X_{t-i} + \sum_{i=1}^{\infty} c_{2i} Z_{t-i} + \overrightarrow{\epsilon_{4t}} + \overrightarrow{\epsilon_{4t}^{E}} + \overrightarrow{B_4(\mathcal{L})\epsilon_{4t}^{L}} \\ Z_t &= \sum_{i=1}^{\infty} b_{2i} Z_{t-i} + \sum_{i=1}^{\infty} d_{2i} X_{t-i} + \overrightarrow{\epsilon_{5t}} + \overrightarrow{\epsilon_{5t}^{E}} + \overrightarrow{B_5(\mathcal{L})\epsilon_{5t}^{L}} \end{cases} \tag{4}$$

The noise covariance matrix for the eq. (4) can be represented as

$$S = \begin{bmatrix} \text{var}(u_{4t}) & \text{cov}(u_{4t}, u_{5t}) \\ \text{cov}(u_{5t}, u_{4t}) & \text{var}(u_{5t}) \end{bmatrix} = \begin{bmatrix} S_{44} & S_{45} \\ S_{54} & S_{55} \end{bmatrix}$$

We have defined partial Granger causality in the time domain in our previous paper [16], which reflects the causal influence from Y to X on condition of Z by eliminating the influence of common exogenous inputs and latent variables. It has the following expression:

$$F_{Y \to X|Z}^{(1)} = \ln \left(\frac{|S_{44} - S_{45} S_{55}^{-1} S_{54}|}{|\Sigma_{xx} - \Sigma_{xz} \Sigma_{zz}^{-1} \Sigma_{zx}|} \right) \tag{5}$$

It is interesting to compare $F^{(1)}$ with the definition of the conditional Granger causality $F^{(2)}$ defined by

$$F_{Y \to X|Z}^{(2)} = \ln \left(\frac{|S_{44}|}{|\Sigma_{xx}|} \right) \tag{6}$$

Note that the main difference between the conditional and the partial Granger causality is that in the definition of the conditional Granger causality, the effect of latent and exogenous

variables is not eliminated both in the denominator term $|\Sigma_{xx}|$ and in the numerator term $|S_{44}|$. In our definition of the partial Granger causality, we use the conditional variance in both the denominator $|\Sigma_{xx} - \Sigma_{xz}\Sigma_{zz}^{-1}\Sigma_{zx}|$ and numerator $|S_{44} - S_{45}S_{55}^{-1}S_{54}|$. As a result, the effect of the latent and exogenous variables could be eliminated, as extensively demonstrated in Results section and in [16]. Of particular interests is that the definition of the partial Granger causality has a transparent statistical meaning since it depends on the well understood notation: the conditional variance.

To deal with exogenous inputs and latent variables is one of the central topics in statistics and, as one could expected, there are published results on the topic. At page 353 in [8], for example, the author has raised the issue and gone further at page 355 to define the partial directed correlation. However, our approach is completely different. First of all, the partial Granger causality is based upon the definition of the conditional Granger causality, which is proved to be one of the most widely used Granger causality definition [5] in the literature. The statistical meaning is transparent, as discussed in the paragraph above. Secondly, as also mentioned above, we extend the time domain partial Granger causality to the frequency domain in the next subsection which is one of the most appealing properties of the Granger causality.

3.2 Partial Granger causality: frequency domain

To drive the spectral decomposition of the time domain partial Granger causality, we first multiply the matrix

$$P_1 = \begin{pmatrix} I_k & -S_{45}S_{55}^{-1} \\ \mathbf{0} & I_m \end{pmatrix} \tag{7}$$

to both sides of eq. (4). The normalized equations are represented as:

$$\begin{pmatrix} D_{11}(L) & D_{12}(L) \\ D_{21}(L) & D_{22}(L) \end{pmatrix} \begin{pmatrix} X_t \\ Z_t \end{pmatrix} = \begin{pmatrix} X_t^* \\ Z_t^* \end{pmatrix} \tag{8}$$

with $D_{11}(0) = I_k, D_{22}(0) = I_m, D_{21}(0) = \mathbf{0}, \text{cov}(X_t^*, Z_t^*) = 0$, we note that $\text{var}(X_t^*) = S_{44} - S_{45}S_{55}^{-1}S_{54}, \text{var}(Z_t^*) = S_{55}$. For eq. (3), we also multiply the matrix

$$P = P_3 \cdot P_2 \tag{9}$$

where

$$P_2 = \begin{pmatrix} I_k & \mathbf{0} & -\Sigma_{xz}\Sigma_{zz}^{-1} \\ \mathbf{0} & I_l & -\Sigma_{yz}\Sigma_{zz}^{-1} \\ \mathbf{0} & \mathbf{0} & I_m \end{pmatrix} \tag{10}$$

and

$$P_3 = \begin{pmatrix} I_k & \mathbf{0} & \mathbf{0} \\ -(\Sigma_{xy} - \Sigma_{xz}\Sigma_{zz}^{-1}\Sigma_{zy})(\Sigma_{xx} - \Sigma_{xz}\Sigma_{zz}^{-1}\Sigma_{zx})^{-1} & I_l & \mathbf{0} \\ \mathbf{0} & \mathbf{0} & I_m \end{pmatrix} \tag{11}$$

to both sides of eq.(3). The normalized equation of eq. (3) becomes

$$\begin{pmatrix} B_{11}(L) & B_{12}(L) & B_{13}(L) \\ B_{21}(L) & B_{22}(L) & B_{23}(L) \\ B_{31}(L) & B_{32}(L) & B_{33}(L) \end{pmatrix} \begin{pmatrix} X_t \\ Y_t \\ Z_t \end{pmatrix} = \begin{pmatrix} \epsilon_{xt} \\ \epsilon_{yt} \\ \epsilon_{zt} \end{pmatrix} \tag{12}$$

where $\epsilon_{xt}, \epsilon_{yt}, \epsilon_{zt}$ are independent, and their variances being $\hat{\Sigma}_{xx}, \hat{\Sigma}_{yy}$ and $\hat{\Sigma}_{zz}$ with

$$\begin{cases} \hat{\Sigma}_{zz} &= \Sigma_{zz} \\ \hat{\Sigma}_{xx} &= \Sigma_{xx} - \Sigma_{xz}\Sigma_{zz}^{-1}\Sigma_{zx} \\ \hat{\Sigma}_{yy} &= \Sigma_{yy} - \Sigma_{yz}\Sigma_{zz}^{-1}\Sigma_{zy} - \dfrac{(\Sigma_{yx} - \Sigma_{yz}\Sigma_{zz}^{-1}\Sigma_{zx})(\Sigma_{xy} - \Sigma_{xz}\Sigma_{zz}^{-1}\Sigma_{zy})}{(\Sigma_{xx} - \Sigma_{xz}\Sigma_{zz}^{-1}\Sigma_{zx})} \end{cases}$$

After Fourier transforming eq. (8) and eq. (12), we can rewrite these two equations in the following expression:

$$\begin{pmatrix} X(\lambda) \\ Z(\lambda) \end{pmatrix} = \begin{pmatrix} G_{xx}(\lambda) & G_{xz}(\lambda) \\ G_{zx}(\lambda) & G_{zz}(\lambda) \end{pmatrix} \begin{pmatrix} X^*(\lambda) \\ Z^*(\lambda) \end{pmatrix} \tag{13}$$

and

$$\begin{pmatrix} X(\lambda) \\ Y(\lambda) \\ Z(\lambda) \end{pmatrix} = \begin{pmatrix} H_{xx}(\lambda) & H_{xy}(\lambda) & H_{xz}(\lambda) \\ H_{yx}(\lambda) & H_{yy}(\lambda) & H_{yz}(\lambda) \\ H_{zx}(\lambda) & H_{zy}(\lambda) & H_{zz}(\lambda) \end{pmatrix} \begin{pmatrix} E_x(\lambda) \\ E_y(\lambda) \\ E_z(\lambda) \end{pmatrix} \tag{14}$$

Note that $X(\lambda)$ and $Z(\lambda)$ from eq. (13) are identical with that from eq. (14), we thus have

$$\begin{aligned}\begin{pmatrix} X^*(\lambda) \\ Y(\lambda) \\ Z^*(\lambda) \end{pmatrix} &= \begin{pmatrix} G_{xx}(\lambda) & 0 & G_{xz}(\lambda) \\ 0 & 1 & 0 \\ G_{zx}(\lambda) & 0 & G_{zz}(\lambda) \end{pmatrix}^{-1} \begin{pmatrix} H_{xx}(\lambda) & H_{xy}(\lambda) & H_{xz}(\lambda) \\ H_{yx}(\lambda) & H_{yy}(\lambda) & H_{yz}(\lambda) \\ H_{zx}(\lambda) & H_{zy}(\lambda) & H_{zz}(\lambda) \end{pmatrix} \begin{pmatrix} E_x(\lambda) \\ E_y(\lambda) \\ E_z(\lambda) \end{pmatrix} \\ &= \begin{pmatrix} Q_{xx}(\lambda) & Q_{xy}(\lambda) & Q_{xz}(\lambda) \\ Q_{yx}(\lambda) & Q_{yy}(\lambda) & Q_{yz}(\lambda) \\ Q_{zx}(\lambda) & Q_{zy}(\lambda) & Q_{zz}(\lambda) \end{pmatrix} \begin{pmatrix} E_x(\lambda) \\ E_y(\lambda) \\ E_z(\lambda) \end{pmatrix}\end{aligned} \tag{15}$$

where $\mathbf{Q}(\lambda) = \mathbf{G}^{-1}(\lambda)\mathbf{H}(\lambda)$. Now the power spectrum of X^* is

$$S_{x^*x^*}(\lambda) = Q_{xx}(\lambda)\hat{\Sigma}_{xx}Q'_{xx}(\lambda) + Q_{xy}(\lambda)\hat{\Sigma}_{yy}Q'_{xy}(\lambda) + Q_{xz}(\lambda)\hat{\Sigma}_{zz}Q'_{xz}(\lambda) \tag{16}$$

where $'$ denotes the complex transformation and conjunction. Note that $\hat{\Sigma}_{xx} = \Sigma_{xx} - \Sigma_{xz}\Sigma_{zz}^{-1}\Sigma_{zx}$, the first term can be thought of as the intrinsic power eliminating exogenous inputs and latent variables and the remaining two terms as the combined causal influence from Y on the mediate of Z. This interpretation leads immediately to the definition

$$f_{Y\to X|Z}(\lambda) = \ln \frac{|S_{x^*x^*}(\lambda)|}{|Q_{xx}(\lambda)\hat{\Sigma}_{xx}Q'_{xx}(\lambda)|} \tag{17}$$

Note that according to eq. (8), the variance of X^* equals to $S_{44} - S_{45}S_{55}^{-1}S_{54}$, By the Kolmogrov formula [12] for spectral decompositions and under some mild conditions, the Granger causality in the frequency domain and in the time domain measures satisfies

$$F_{Y\to X|Z} = \frac{1}{2\pi}\int_{-\pi}^{\pi} f_{Y\to X|Z}(\lambda)d\lambda \tag{18}$$

The dependence of partial Granger causality on the coefficient of VAR model is quite complex, as discussed in supplemental material I.

4 Discussion

We have presented a study on the frequency decomposition for the partial Granger causality. The defined partial Granger causality and its frequency domain decomposition is successfully applied to toy models and experimental data.

4.1 Partial Granger Causality and its frequency domain decomposition

As expected, in the literature various definitions of the Granger causality in the frequency domain have be introduced. For more than three time series, Kalminski and Blilowska [27] proposed a full multi-variate spectral measure, called directed transfer function (DTF), which is used to determine the directional influences between any given pair of variables in a multivariate data set. Sameshima and Baccalá [2] introduced PDC to detect direct influence of multivariables. Actually Geweke [11] has early introduced the conditional Granger causality to infer the original direct relationship between multi-variable time series, as recently reviewed in [12, 6, 5]. In [11] both a time domain measure, consistent with that of Granger, and its frequency decomposition were given. However, when the exogenous inputs or latent variables are present, the conditional Granger causality fails to pick up the correct causal relationship while the partial Granger causality we defined remains robust against the exogenous input and latent variables (see Fig. 1), as pointed out in our previous paper[16]. One of the key properties of the conditional Granger causality of Geweke's formulation is that the summation of the Granger causality in the frequency domain equals the Granger causality in the time domain. This is due to the Kolmogrov equation for frequency decompositions. Both PDC and DTF lack this property and the inferred structures could be simply misleading. Here we follow the idea of Geweke's formulation and the partial Granger causality in the frequency domain is given.

One of our aims of the current paper is to present a method to correctly calculate the Granger causality when there are latent variables and exogenous inputs. Our results on toy models have demonstrated that the Granger causality defined here is robust against latent variables and exogenous inputs, in comparison with the quantities such as the conditional Granger causality etc. The other aim is to demonstrate that an *ad hoc* definition of the causality such as PDC in the frequency domain could be misleading. It usually yields contradictionary results between the time domain Granger causality and the frequency domain Granger causality.

4.2 HeLa gene network

Due to the limitation of HeLa microarray data (sampling rate is one hour), we are not able to assess the fast dynamical activity which occurs at a minute scale. It is pointed out in [18] that there are two pathways in NF-κB circuit: one is canonical (fast time scale, minutes) and the other is non-canonical (slow time scale, hours or days). The canonical pathway involves NEMO and is faster than the non-canonical pathway which does not involve NEMO. Our results contradict the conclusions above. The non-canonical pathway does involve NEMO, although it exhibits a slow dynamics. Of course, we do not exclude the possibility that the causality between IKKα and NEMO is due to the crosstalk between canonical and noncanonical pathways. However, one thing is certain. The claim that 'It is important to note that non-canonical activation of NF-κB appears to lack highly dynamic control' [18] seems untrue. NF-κB circuit clearly shows a tri-frequency activity and the causality between each gene is strong or significant.

4.3 Gamma, beta and theta rhythms

Gamma rhythms occur during persistent, self-sustained activity and are a hallmark of cortical activity during sensory processing and cognition. Beta oscillatory activity is often observed to be synchronized between various parts of sensorimotor cortex. Theta-frequency activity is observed during some short term memory tasks and reflects the on-line state of the hippocampus; one of readiness to process incoming signals [3]. In out data, although theta wave is observable for most channels (see Fig. 4 **B**), they are synchronous at around 300 ms, which is more or less the time of the evolved field potential. In conclusion, there are different frequencies in the recorded brain activity and their interactions give rise to cognitive functions.

Acknowledgements

We are grateful to the referees for their useful comments and bring our attention to the references [10, 7, 9, 8]. J.F. was partially supported by grants from UK EPSRC (EP/C51338X),

(EP/D051916), (GR/S30443) and BBSRC (BB/E005802).

References

[1] Baccalá L, Sameshima K, Ballester G, Valle AC and Timo-Iaria C. (1998) Studying the Interaction between Brain Structures via Directed Coherence and Granger Causality. *Appl. Signal Process*, **5**: 40-48.

[2] Baccalá L and Sameshima K. (2001) Partial Directed Coherence: a New Conceptin Neural Structure Determination. *Biological Cybernetics*, **84**: 463-474.

[3] Buzsaki G (2002) Theta oscillations in the hippocampus. *Neuron 33*(3):325-40.

[4] Canolty RT, Edwards E, Dalal SS, Soltani M, Nagarajan SS, Kirsch HE, Berger MS, Barbaro NM, and Knight RT. (2006) High gamma power is phaselocked to theta oscilltions in human neocortex. *Science*, **313**: 1626-1628.

[5] Chen YH, Bressler SL, and Ding MZ. (2006) Frequency Decomposition of Conditional Granger Causality and Application to Multivariate Neural Field Potential Data. *J Neurosci Methods*, **150:** 228-237.

[6] Ding MZ, Chen YH, and Bressler SL. (2006) Granger Causality: Basic Thoery and Application to Neuroscience. *Handbook of Time Series Analysis*, ed. Schelter,B., Winterhalder,M.,Timmer,J. Wiley-VCH Verlage, 451-474.

[7] Eichler M (2005) A graphical approach for evaluating effective connectivity in neural systems *Phil. Trans. Royal. Soc. B* **360**: 953-967.

[8] Eichler M (2006) Graphical modelling of dynamic relationships in multivariate time series, *Handbook of Time Series Analysis*, ed. Schelter,B., Winterhalder,M.,Timmer,J. Wiley-VCH Verlage, 335-372.

[9] Valdes-Sosa PA, Sanchez-Bornot JM, Lage-Castellanos A, Vega-Hernandez M, Bosch-Bayard J, Melie-Garcia L, Canales-Rodriguez E (2005) Estimating brain func-

tional connectivity with sparse multivariate autoregression, *Phil. Trans. Royal. Soc. B* **360**: 969-981.

[10] Ghahramani Z. (1998) Learning dynamic Bayesian networks, in C.L. Giles and M. Gori (eds.) *Adaptive Processing of Sequences and Data Structures*. Lecture Notes in Artifical Intelligence, 168-197, Berlin: Springer-Verlag.

[11] Geweke J. (1982) Measurement of Linear Dependence and Feedback Between Multiple Time Series. *Journal of the American Statistical Association*, **77**: 304-313.

[12] Geweke J. (1984) Measures of Conditional Linear Dependence and Feedback Between Time Series. *Journal of the American Statistical Association*, **79**: 907-915.

[13] Gourierous C and Monfort A. (1997) *Time Series and Dynamic Models*, cambridge University Press, London.

[14] Granger C. (1969) Investigating Causal Relations by Econometric Models and Cross-spectral Methods. *Econometrica*, **37**: 424-438.

[15] Granger C. (1980) Testing for Causality: A Personal Viewpoint. *Journal of Economic Dynamics and Control*, **2**: 329-352.

[16] Supplemental material II, also available at http://www.dcs.warwick.ac.uk/~feng/papers/supplemental_material_II.pdf.

[17] Gourevitch B, Le Bouquin-Jeannes and Gaucon G. (2006). Linear and nonlinear causailty beteween signals: methods, examples, and neurophysiological applications. *Biol. Cybern.*, **95**: 349-369.

[18] Hoffmann A and Baltimore D. (2006) Circuitry of nuclear factor κB signalling. *Immunological Reviews*, **210**: 171-186.

[19] Hoffmann A, Levchenko A, Scott ML and Baltimore D. (2002) The IκB-NFκB signaling module: temporal control and selective gene activation. *Science*, **298**: 1241-1245.

[20] Horton PM, Bonny L, Nicol AL, Kendrick KM and Feng JF. (2005) Applictions of multi-variate analysis of variances (MANOVA) to multi-electrode array data. *J Neurosci Methods*, **146**: 22-41.

[21] Horton PM, Nicol AU, Kendrick KM and Feng JF. (2007) Spike sorting based upon machine learning algorithms (SOMA). *J Neurosci Methods*, **160**: 52-68.

[22] Hosoya Y. (1991) The decomposition and measurement of the interdependency between second-order stationary process. *Probability Thoery and Related Fields*, **88**: 429-444.

[23] Hosoya Y. (2001) Elimination of third-series effect and defining partial measures of causality. *J of Time Series*, **22**:537-554

[24] Ishai A, Ungerleider LG, Martin A, Schouten JL and Haxby JV. (1999) Distributed representation of objects in the human ventral visual pathway. *PNAS*, **96**:9379-84.

[25] Kreiman G, Hung CP, Kraskov A, Quiroga RQ, Poggio T and DiCarlo JJ. (2006) Object selectivity of local field potentials and spikes in the macaque inferior temporal cortex. *Neuron*, **49**:433-45.

[26] Jeong SJ, Radonovich M, Brady JN and Pise-Masison CA. (2004) HTLV-I Tax induces a novel interaction between p65/RelA and p53 wich results in inhibition of p53 transcirptional activity. *Blood*, doi:10/1182/blood-2003-12-4174.

[27] Kaminski M, Ding MZ, Tryccolo WA and Bressler SL. (2001) Evaluating causal relations in neural system: Granger causality, directed transfer function and statistical assessment of significance. *Biol. Cybern*, **85**: 145-157.

[28] Kim J, Zhu W and Chang L. (2007) Unified Structural Equation Modeling Approach for the Analysis of Multisubject, Multivariate Functional MRI Data. *Human Brain Mapping*, **28**: 85-93.

[29] Krishna S, Jensen MH and Sneppen K. (2006) Minimal model of spiky oscillations in NF-κB signaling. *PNAS*, **103**: 10840-10845.

[30] Longo D and Hasty J. (2006) Dynamics of single-cell gene expression. *Molecular Systems Biology*, **2**: 64-75.

[31] Lutkepohl H. (1993) *Introduction to Multiple Time Series Analysis*, Springer-Verlag.

[32] Nelson DE, et al. (2004) Oscillations in NF-κB signaling control the dynamcis of gene expression. *Science*, **306**: 704-708.

[33] Pearl J. (1998) *Causality: Models, Reasoning, and Inference*. Cambridge University Press: Cambridge, UK.

[34] Whitfield ML, Sherlock G, Saldanha AJ, Murray JI, Ball CA, Alexander KE, Matese JC, Perou CM, Hurt MM, Brown PO and Botstein D. (2002) Identification of genes periodically expressed in the human cell cycle and their expression in tumors. *Mol Biol Cell.*, **13**: 1977-2000.

[35] Wiener.N. (1956) *The theory of prediction*. In: Beckenbach EF (ed) Modern mathematics for engineers, chap 8. McGraw-Hill, New York.

[36] Wu JH, Kendrick KM and Feng JF. (2007) Detecting Correlation Changes in Electrophysiological Data. *Journal of Neuroscience Methods*, **161**: 155-165.

[37] Wu JH, Kendrick KM and Feng JF. (2007) Detecting Hot-Spots in Multivariates Biological Data. *BMC Bioinformatics*, **8**: 331.

[38] Wu JH, Liu XG and Feng JF. (2008) Detecting causality between different frequencies, *J. Neuroscience Methods*, **167**: 367-375.

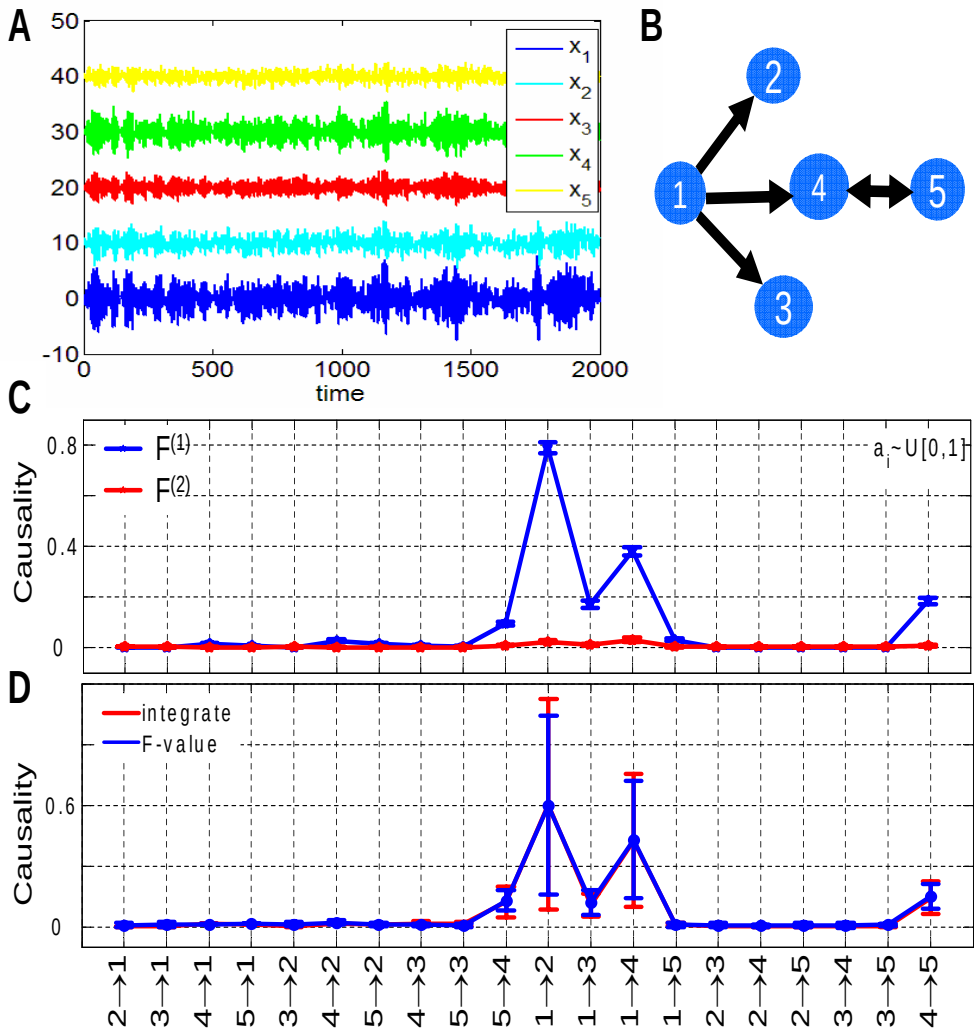

Figure 1: (**A**):Traces of the time series we considered in Example 1 when $a_i \sim U[0,1], b_i = 2, c_i = 5, i = 1 \cdots, 5$. x_2, x_3, x_4 and x_5 are shifted upward for visualization purpose. (**B**): The causality structure is plotted. (**C**): Comparison of the partial Granger causality $F^{(1)}$ and the conditional Granger causality $F^{(2)}$ when $a_i \sim U[0,1]$. It is obvious that $F^{(2)}$ fails to pick up the correct relationship while the inferred relationship from $F^{(1)}$ is consistent with the true structure(**B**). (**D**): Comparison of the partial Granger causality in the time domain and frequency domain when $a_i \sim U[0,1], i = 1, \cdots, 5$ in Example 1. Blue line represents the case of time domain, red line is the integral of the frequency domain in the interval $[-\pi, \pi]$.

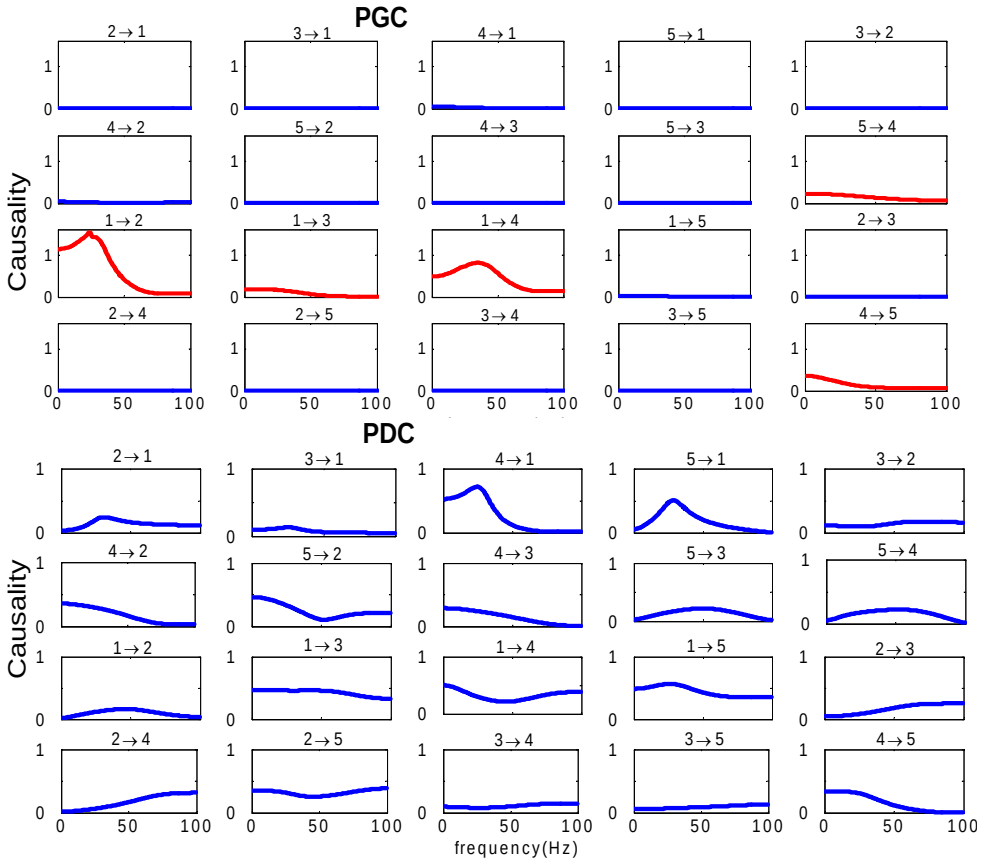

Figure 2: Comparison of the frequency decomposition of all 20 kinds of relationship between the partial Granger causality (PGC) and PDC in Example 1 with $a_i \sim U[0,1], b_i = 2, c_i = 5, i = 1, \cdots, 5$. Upper panels are the results of PGC, bottom panels are the results of PDC.

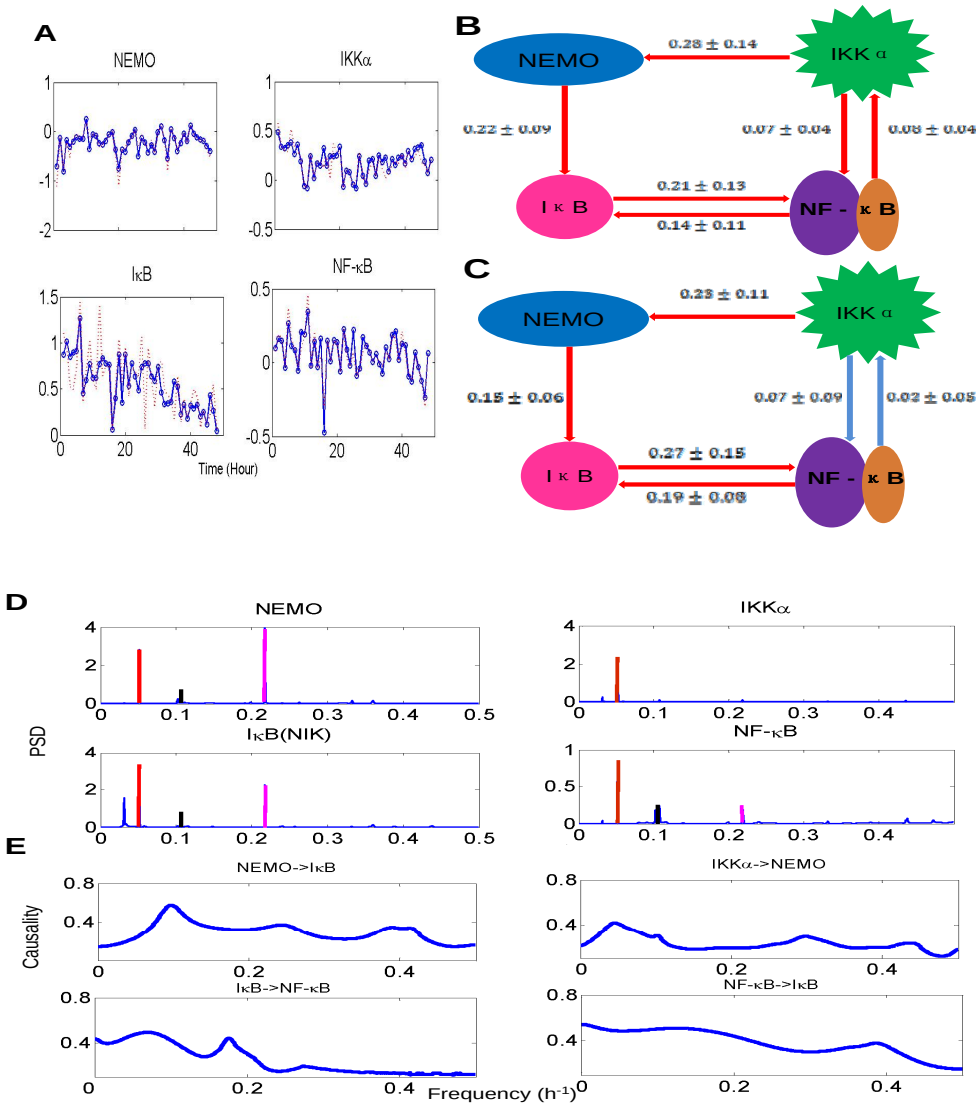

Figure 3: (**A**) Gene expression profile plot of actual data and fitted data by AR model to the NF-κB, NEMO, IKKα, IκB genes. A network is composed based on calculated time domain causality for gene module NF-κB, which contains NF-κB, NEMO, IKKα, IκB genes. (**B**) is constructed based on pairwise Granger causality method, and (**C**) is constructed based on PGC method. According to the confidence interval, two connections become insignificant after partial influence is taken into account. (**D**) Power spectrum density (PSD) for IKKα, NEMO, IκB and NF-κB genes. There is only one frequency at 16 hours in IKKα, but there are two prominent frequencies for NEMO, IκB and NF-κB at 16 hours and 4 hours. (**E**) Frequency domain causality for IKKα, NEMO, IκB and NF-κB genes.

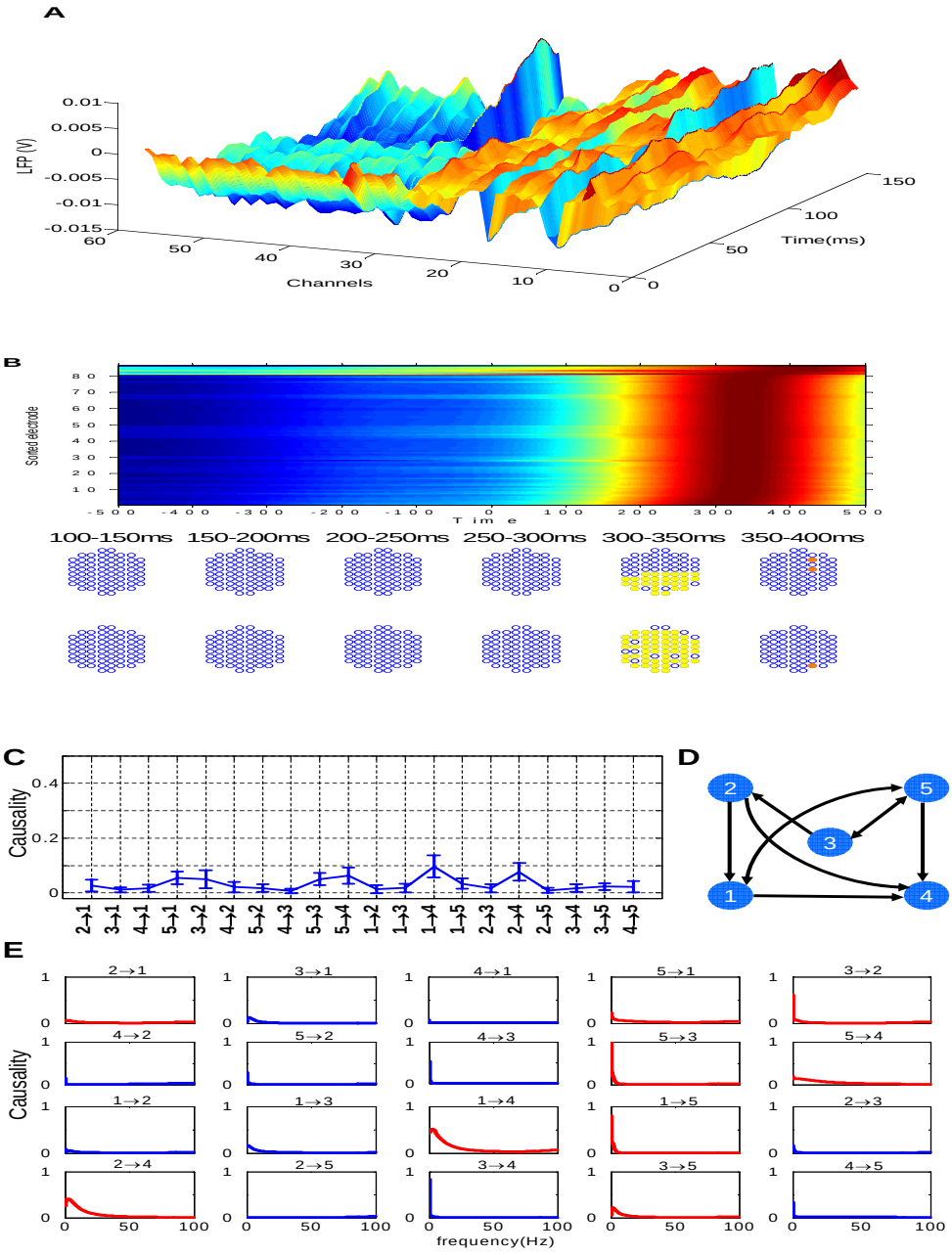

Figure 4: Results for sheep data. (**A**) Local field potential recorded from 64 channels. Time 0 is the starting point of stimuli. (**B**) Spatial-temporal pattern of theta power distribution (-500 to500 ms) across the recording array for one experimental session in response to face presentation. Electrodes are arranged by the latency of the normalized theta power. The electrodes with increased power are marked by the filled colour on the electrode grid in different time slots of 50 ms in the duration 100-400 ms. (**C**) Partial Granger causality of all possible relationship in time domain. (**D**) The inferred structure from experimental data in the time domain. (**E**) The frequency decomposition of all possible relationship is consistent with the structure inferred from time domain.

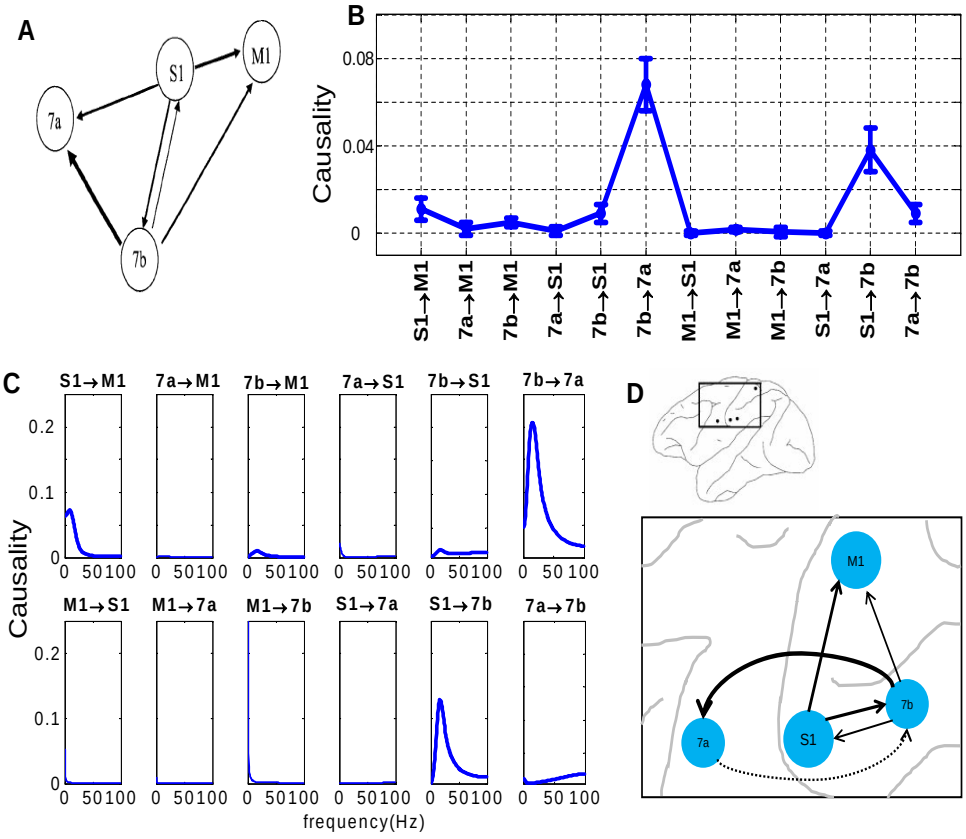

Figure 5: Results for monkey data. (**A**) Pairwise Granger causality of all possible relationships. (**B**) The partial Granger causality in the time domain. (**C**) Frequency decomposition of all possible relationships. (**D**) The inferred structure from experimental data. The four areas in the brain are marked in the upper trace and the detailed interactions are shown in the bottom trace. The dashed line indicates the additional interaction found using partial Granger causality.